Evaluation of the solar thermal storage of fluidized bed materials for hybrid solar thermo-chemical processes

Evaluation of the solar thermal storage of fluidized bed materials for hybrid solar thermo-chemical processes

Su Been Seo[a], Hyungwoong Ahn[b], Eun Sol Go[c], Lih Jie Jester Ling [a], Nancy Julius Siambun[d], Young-Kwon Park[e*], See Hoon Lee[a,c*],

[a]Department of Mineral Resources and Energy Engineering, Jeonbuk National University, 567 Bakeje-daero, Deokjin-gu, Jeonju, Republic of Korea

[b]Institute for Materials and Processes, School of Engineering, The University of Edinburgh, Robert Stevenson Road, Edinburgh EH9 3FB, United Kingdom

[c]Department of Environment & Energy, Jeonbuk National University 567 Baekje-daero, Deokjin-gu, Jeonju, Republic of Korea

[d]Mechanical Engineering, Faculty of Engineering, Universiti Malaysia Sabah, Jalan UMS, 88400 Kota Kinabalu, Sabah, Malaysia

[e]*School of Environmental Engineering, University of Seoul, Seoul 02504, Korea*

*Co-Corresponding author: catalica@uos.ac.kr

*Co-Corresponding author: donald@jbnu.ac.kr

ABSTRACT

The use of solid particles as a solar energy transport and storage medium overcomes the intermittency issues for solar energy and is advantageous for the development of a hybrid process that integrates biomass and solar thermal energy. In this study, lab-scale experimental equipment consisted of bubbling fluidized bed (55mm I.D. and 200mm height) with direct irradiated solar thermal storage was designed and constructed. Sand, alumina (Al), and silica carbide (SiC) particles with 3 different particle sizes (130μm, 250μm, and 370μm) were used as a solar thermal storage medium in the fluidized bed. Due to higher absorption and emissivity properties, the solar thermal efficiency of SiC was higher than those of sand and Al. As the gas velocities in the bubbling fluidized bed increased from the initial minimum fluidization velocity (Umf) to 2 Umf, the temperature differences between upper bed and lower bed decreased from 470°C to 35°C because of vigorous solid mixing and heat transfer. Also, the increase of average particle size resulted in the decrease of solid heat storage and the increase of gas heat storage due to the differences of specific surface area and gas velocity. Therefore, the energy transported and stored according to the size of silicon carbide was the highest at 370 μm, and the receiver efficiency was 21.38%.

Keywords: Solar thermal energy; Particle receiver; Energy storage; Fluidized bed; Silicon carbide

1. Introduction

Building a low-carbon society with the aim of reducing greenhouse gas emission is to be addressed urgently as one of the gravest societal issues [1]. Thermochemical conversion processes integrating with multiple renewable energy resources such as solar heat [2], biomass [3], and waste [4] can simultaneously solve the disadvantages of fossil fuels that cause environmental pollution and the intermittency issues of renewable energy.

Solar energy is considered one of the promising energy sources because it is sustainable and environmentally beneficial compared to other energy sources [2, 5, 6]. Concentrated solar power (CSP) system is a power generation method in which solar energy is collected and used directly as a heat source for the power cycle. Since the operating principle of a CSP system is the same as that of a thermal power plant, it can be integrated with an existing thermal power plant. Therefore, it has been recognized as a promising technology that is applicable to sustainable power generation of various scales [7, 8]. To overcome the intermittent characteristic of solar energy, a variety of energy storage devices heat transfer fluids (HTF) have been developed and tested so far. Liquid phase molten salt has been mainly used as a HTF to transfer or store thermal energy in solar power generation systems. However, the maximum temperature of a molten salt for thermal storage is limited to 600 °C due to its corrosiveness that increases with the temperature [9]. A fluidized bed system using solid particles has been proposed as an alternative to the liquid molten salt [10, 11]. Solid HTF particles have several advantages, such as higher operating temperature above 1000°C, higher heat capacity than HTFs in liquid or gas phases, and capability of directly absorbing condensed solar thermal energy [12]. Therefore, it enables a high-efficiency power cycle and improves the commercial competitiveness of the CSP system.

A fluidized bed with smooth mixing of solid particles and good heat transfer characteristics has been utilized in various thermochemical processes so far [13-16]. A fluidized bed process is being actively studied for integration with solar energy, and solid particles are used as a carrier or storage medium for heat energy [2, 17]. A variety of integrated solar direct irradiation fluidized bed receivers using solid particles have been proposed, and some prototypes have been tested at the laboratory scale [18, 19]. It is crucial finding solid particles best suited for solar direct irradiation fluidized bed receiver and understanding the heat transfer process involved. Briongos et al. [20] selected silicon carbide and zirconia as solid particles to investigate the heat transfer process and solid convection occurring in a bubble fluidized bed exposed to direct sunbeams. Diaz-Heras et al. [21] studied the effect of physical properties of solid particles on the performance of high temperature fluidized beds with silicon carbide, silica sand, or carbo accucast ID50. They studied the effects resulting from the changes in the composition, structure, and

properties of these solid particles in different thermal and fluidization processes.

Most of the experiments mentioned above were conducted with the aid of Xenon lamp to simulate the solar thermal heat, not in actual outdoor conditions where the solar radiation varies with time. It is difficult to evaluate the suitability and actual performance of a solar thermal system in case it was integrated with an existing thermo-chemical conversion process. Therefore, there is a lack of information on the efficiency of solar thermal storage and transfer through heat-absorbing particles in the fluidized bed under actual outdoor conditions. In this study, several particles that can absorb, store, and transfer solar thermal energy were selected and their solar thermal storage efficiencies were investigated through a fluidized bed receiver which was operated under outdoor conditions. In addition, the axial temperature profile of the fluidized bubble bed were investigated with the particle sizes of SiC and gas velocities. The system efficiencies were calculated from the extent of particle temperature change. Fluidized bed receiver tested in this study paves a way to overcome the limitations of solar energy and increase the share of renewable resources in the energy system. It can also be used as a design basis for a hybrid fluidized bed process integrated with solar energy storage to achieve carbon negative emission power generation with the use of biomass resources.

2. Experimental method

2.1 Lab-scale solar thermal storage system

A solar thermal storage equipment based on a fluidized bed was designed to store solar thermal energy using various particles. The Direct Normal Insolation (DNI) is an indispensable indicator to quantify the solar energy received per unit area by a surface. In this paper, an experiment was conducted based on the clearness index and DNI in Jeonju, Korea. The solar power meter (SPM-1116SD model, Lutron Co.) was attached to the first reflecting mirror, and the direct solar radiation from the sun was measured in real time and recorded on the SD card (See Fig. 1). The lab-scale solar integrated fluidized bed process consisted of a first reflecting mirror, a Fresnel lens, a second reflecting mirror, a lab-scale bubbling fluidized bed, and a mass flow controller (MFC) to alter the air flow into the column. Besides, a focal lens was installed to prevent scattering of solar radiation and to concentrate the solar radiation on the surface of the bed in the receiver. The details of equipment used for the system configuration are shown in Fig. 1.

A fresnel lens with a 92% transmittance was installed to focus the sunbeam irradiation into one focal point. The fresnel lens has dozens of inclined projections with different inclination angles constructed on its aperture. It is

thinner and has a shorter focal length than a convex lens. Solar mirror films (models 1100, 3M) were used for the first and second reflecting mirror, which maximize the reflection efficiency of sunbeams up to a total solar reflectance of 94%. The sizes of the first and second reflecting mirror were 510 mm x 910 mm and 200 mm × 200 mm, respectively, and the distance between the first reflecting mirror and the Fresnel lens was selected as 1.2 m. For the first and second reflecting mirrors, the angle can be adjusted according to the position of the sun to maximize the sunbeams sent to the receiver. To prevent light scattering, a pyrex focal lens (I.D. 50 mm, focal length 200 mm) was installed on the top of the receiver as the sunbeams collected by the Fresnel lens is reflected by the second reflecting mirror.

Fig. 2(a) shows a diagram of the bubbling fluidized bed receiver used in the process. To measure the temperature of the inlet gas, the outlet gas, and the particle temperature in bed, K-type thermocouples were installed at different locations of the receiver. As shown in Fig. 2(b), the main column with internal diameter of 55 mm and height of 200 mm was installed with several temperature conductors (TC) that measure the temperature of the bed at a height of 20 mm, 70 mm, and 120 mm of the main column. Fluidizing air is introduced into the receiver and its flowrate is measured by a mass flow meter. The flow rate of fluidizing gas was determined based on the minimum fluidization velocity of the particles and the cross-sectional area (23.76 cm^2) of the receiver. The fluidized bed receiver is made of stainless steel and well insulated. A quartz window with high transparency was installed at the top of the column to obtain high transmittance for irradiation of sunbeams while ensuring a sealed close system of the receiver. The quartz window has a solar weighted transmittance of 93% and can be used for a long time at a temperature of 1100–1200 °C [22]. The wool is used as an insulating material, covering the surface of the receiver to minimize heat loss from the outside. While sunbeams were injected into the receiver, the temperature profile of bed particles along the fluidized bed was measured with the TCs installed on the receiver. The temperature changes of the fluidizing gas were observed at the outlet and inlet TCs of the receiver in order to evaluate how efficient the heat transfer between solid particle and gas were. The temperature of each TCs on the reactor was stored in a computer.

The second experimental rig of a lager scale was built with new fresnel lens of about twice the diameter of old fresnel lens used in the initial experiment. The overall system configuration of the second equipment is shown in Fig. 3. For the scale-up model, a fresnel lens of 1000 mm x 1000 mm was selected, and the distance between the Fresnel lens and the second reflecting mirror was adjusted to 1000 mm. The size of the first reflecting mirror was set to 1200 mm x 1230 mm, and the size of the second reflecting mirror remains the same (200 mm x 200 mm).

The fluidized bed particle receiver, pyrex focal lens, solar power meter, mass flow controller (MFC), and solar mirror film (models 1100, 3M) were also used in the same way as they were in the initial experiment.

2.2 Solar storage material

Sand, Al, and SiC particles were selected for solar thermal storage and fluidized bed formation in the lab-scale solar storage receiver. To determine the particle size suitable for the bubbling fluidized receiver, the particle classification standard with respect to the particle density and size suggested by Geldart [23] was referred to. As a result, all the selected particles belong to B group in the Geldart particle classification [23, 24] as shown in Fig. 4. Because B group particles was highly recommended for the fluidized bed, all the selected particles were considered suitable for the experimental operation. The physical properties of each particle are compared and shown in Table 1 [25-27].

As can be seen, silicon carbide and alumina oxide are also selected for solar thermal storage as they have very high melting points and great heat capacity and thermal conductivity compared to sand which has commercially been used in fluidized bed processes. Therefore, they can be applied to fluidized bed power plants conventionally operating at 800-900 ℃. Since the density of both particles is higher than that of sand, it can be inferred that the minimum fluidization velocity of both particles should increase compared to sand. Kim et al [25]. compared the attrition and heat transfer characteristic of SiC and Al with sand through experiments as a heat storage medium in the fluidized bed process integrated solar. As a result, it was confirmed that the attrition resistances of SiC and Al was superior to that of sand, and the heat transfer coefficient was also similar to or greater than that of sand ranging 125~152 W/m^{2}K.

2.3 Equations

It was assumed that the sunbeams injected into fluidized bed process would be stored in both particle and gas. This was because the particles heated by sunbeams subsequently transferred heat to the fluidizing air injected into the receiver. According to the specific heat data in Table 2, the energy stored in gas and particles per unit time was calculated by the following Eq. (1), (2) [28].

$$Q_{particle} = m_p C_p (T_b(t) - T_0) \tag{1}$$

$$Q_{gas} = U_{mf} \rho_g \left(\frac{\pi}{4} {d_{bed}}^2\right) C_g \left(T_{g.0} - T_{g.i}\right) \tag{2}$$

Where, $Q_{particle}$ and Q_{gas} are heat energy per unit time of the particle and gas respectively, m_p is mass of

particles in the bed, U_{mf} is minimum fluidization velocity of gas, ρ_g is density of gas, d_{bed} is receiver diameter, C_p, C_g are specific heat of gas and particle respectively, T_b is temperature of particles in bed, T_0 is environment temperature, $T_{g.0}$ is outlet temperature of gas and $T_{g.i}$ is inlet temperature of gas.

The experiment involved two stages. The initial stage was conducted with 100g of particles injected into the column to find the optimum particles among sand, SiC, and Al with respect to the highest achievable temperature of the particles. The ensuing stage involved scaled up experiment. 500g of the particle selected from the initial stage was injected into the scale-up equipment with the size of particle varied. The temperature of the particles along to the column height was observed and the temperature of the gas was measured. The receiver efficiency was obtained using the following equations [17, 29].

$$\eta_{rec} = \frac{Q_{particle} + Q_{gas}}{Q_{solar}} \tag{3}$$

$$Q_{solar} = I_{DNI} A_{Fresnel} \rho_{mirror} \tau_{l,Fresnel} \tau_{l,focal} \tau_{quartz} \tag{4}$$

Where, Q_{solar} is solar energy per second obtained by the solar collector system, I_{DNI} is intensity of direct normal irradiance, $A_{Fresnel}$ is area of Fresnel lens, ρ_{mirror} is reflectance of the second reflect mirror, $\tau_{l,Fresnel}$ is transmittance of fresnel lens, $\tau_{l,focal}$ is transmittance of focal lens and τ_{quartz} is transmittance of transparent quartz plate.

3. Result and discussion

3.1 Optimal particle selection

A series of experiments to evaluate the solar thermal storage using solid particles were carried out for each particle. To find the maximum performance of each particles, the experiments were only evaluated when a DNI of 800 W/m^2 or more was recorded. Sand, SiC and Al particles were injected at 100 g each and tested at a rate of 1.5 minimum fluidization velocity (Umf). The heat energy rate that can be stored in the solid particles was calculated by Eq. (1) based on the extent of rising temperature for about 3 minutes, and the results were sand (3.3 W), Al (5.3 W), and SiC (8.9 W) in the increasing order of the heat storage power. However, the thermal efficiency of the receiver was estimated by Eq. 5 and they are shown in Fig. 5 because of DNI variation caused by the difference in sunlight between the test dates.

The thermal efficiency of the receiver was higher sand (2.39%), Al (4.63%), and SiC (6.52%), the order of which was the same as the order of the heat storage power of each particle. The higher thermal efficiency obtained by SiC particle was mainly due to the high emissivity of SiC particles as shown in Table 1. This was because the

absorption rate was assumed to be equal to the emissivity. The emissivity of SiC particles is about 1.8 times higher than that of sand. It is meant that SiC could be superior to sand in case of solar thermal storage. In addition, it can be seen from previously published literature that SiC particles have higher attrition resistances and thermal conductivity than sand particles [25]. Therefore, SiC is considered as an optimal particle capable of storing solar heat more efficiently than sand. However, the heat storage power and efficiency of SiC particles with the initial configuration was quite low, so there is a need to revise the configuration used.

3.2 Evaluation of solar thermal storage efficiency by particle

The scale-up equipment was built in order to achieve higher solar thermal storage and efficiency by means of expanding the size of the fresnel lens in the initial configuration. The initial configuration had confirmed that SiC would have the highest energy storage efficiency of the three candidates. The ensuing experiments were performed using SiC particles of different sizes in the scale-up configuration since an appropriate particle size is an important parameter to optimize for achieving excellent solar energy storage efficiency.

As the equipment became larger, the quantity of particles injected into the receiver increased to 500 g accordingly. The formation of gas bubbles and their upward flow in the bubbling fluidized bed generates a flywheel effect, forming a better mixing and enhancing convective heat transfer between gas and particles [17, 30]. As the extents of mixing and heat transfer tend to be affected greatly by gas flowrate or gas velocity, it is necessary to evaluate the temperature profiles over the entire fluidized bed under different gas velocities. Fig. 6 shows the axial temperature profile of a bubble fluidized bed with different SiC particle sizes (a) 130 μm and (b) 250 μm at different gas velocities. The gas velocities are expressed in the ratio of the actual gas velocity to the minim fluidized gas velocity in Fig. 6. As can be seen, the temperature difference between the upper and lower parts of the bed was as large as about 470 ℃ when it was tested at the velocity ratio of 1 with 130 μm SiC. However, as the gas velocity ratio increased to 2, the upper bed temperature is 309 ℃ and the lower bed temperature is 274 ℃, which indicates that solids were well mixed at an average temperature about 300 ℃.

In the experiment using 250 μm SiC, the temperature difference between the upper and lower parts of bed at 1 Umf was about 453 ℃, and as the gas velocity increased, the average temperature of the bed was about 180 ℃. These experiments showed that the bed temperature profiles became uniform due to vigorous mixing with the gas velocity increasing, and this trend was observed in both experiments where the SiC sizes were varied. Flamant et al. [31] and Matsubara et al. [32] also reported that as the gas velocity increased, the particles in the fluidized bed were mixed more efficiently and as a result the temperature profile became more uniform along the bed height.

The experiment results showed clearly that as the gas velocity increased, the average temperature of the well-mixed region decreased. It was also found that the performances of the 130 μm SiC case were superior to those of 250 μm SiC with respect to solid mixing and temperature rising. This is because presumably the heat transfer rate between the particles and gas was greater with 130 μm SiC due to the larger specific surface.

The solar thermal storage experiments in a bubbling fluidized bed were conducted to see the effect of the particle size on the solar thermal storage efficiency at the gas velocity of 1.5 Umf. In these experiments, the temperatures of fluidizing gas were measured at the fluidized bed outlet for 5000s for the outset. The outlet gas temperature and the gas velocity are shown in Fig. 7. The solid lines indicates the temperature of outlet gas and particle, and the broken line is the temperature difference between the inlet and the outlet gases. As shown in Fig. 7(a), the gas temperature at the fluidized bed outlet with the particle size of 370 μm reached 228 °C (solid line) around 5000 s. As can be seen from Fig. 7(a), the gas flow rate decreases as the size of the solid particles decrease under the same conditions of 1.5 Umf. Therefore, the smaller the particle size, the longer the residence time of the gas on the freeboard would be, which might result in greater heat loss through the upper light transmission window. As shown in Fig. 7(b), the ΔTp in the bed reached up to 400, 321, and 203 °C with the particle size of 130 μm, 250 μm, 370 μm, respectively. Unlike the gas, ΔTp increased as the size of the particles decreased. Since the large specific surface area of the particles increases the mutual heat transfer rate between the particles, it was found that the smaller the particle size, the greater the influence of the temperature applied by solar thermal.

Fig. 8 shows the energy stored in the particle or carried by the gas stream for different particle sizes. It also shows the DNI on the date when each particle was tested. The average DNI recorded for testing was 1021 W/m^2 for the 130 μm experiment, 970 W/m^2 for the 250 μm experiment, and 1028 W/m^2 for the 370 μm experiment. The solid and broken lines represent the energy stored in the particles and the accumulated energy carried by the gas flowing through the fluidized bed, respectively. In the case of 130 μm, it was confirmed that the energy stored in the particles was greater than the energy carried by the gas, and in the case of 250 and 370 μm, the energy carried by the gas was greater than the energy stored in the particles. Therefore, the larger the particle size, the smaller the energy stored in the particle would be. However, the overall energy efficiency may be improved by the increasing particle size because the gas flow rate has to increase to get the particles fluidized.

Based on the temperature recorded at 5000 s, the total energy stored in both gas and solid phases was calculated by summing the heat energy stored in the gas flowing through the bed and the particles. The efficiency of solar thermal storage in comparison to the provided solar heat was affected greatly by the particle size as shown in Fig. 9. The receiver efficiencies were 8.63% (130 μm), 12.92% (250 μm), and 21.38% (370 μm). At 370 μm, the

receiver efficiency was about 2.48 times higher than 130 μm mainly due to the amount of heat carried by gas being the greatest of all.

The amount of the solar energy required to obtain the target temperature of the particles is shown in Fig. 10. Only the energy stored in SiC particles was considered at the scale of 500 g used in the experiment. The required solar energy was estimated at the time of exposure to sunbeams of 1000, 2000, 3000, and 4000 s. To obtain a temperature of 800 ℃, about 418 W of solar thermal energy was required in case that the exposure time of sunbeams to the particles was only 1000 s. On the contrary, only 105 W of solar thermal energy would be required if the exposure time was 4000 s. Therefore, the shorter the exposure time of the solid particles to the sunbeams, the larger solar energy would be required to obtain the same temperature of the particles.

4. Conclusions

Lab-scale experimental equipment was built to see the feasibility of a direct irradiation particle receiver for storage and transport of solar thermal energy. The results were, sand (2.39%), Al (4.63%), and SiC (6.52%) in the increasing order of efficiency, because SiC particles have good absorption rate, attrition resistances, and thermal conductivity. And it was found that the bed temperature became uniform due to vigorous mixing with the gas velocity increasing . Also, the smaller the particle size, the greater the heat transfer rate would be due to the larger specific area of the particle. The energy stored in the particles was greater than the energy carried by the gas in the case of 130 μm particle size, while the energy carried by the gas was more influential than the energy stored in the particles in case of 250 and 370 μm particle size. Based on this result, the calculated receiver efficiencies were 8.63% (130 μm), 12.92% (250 μm) and 21.38% (370 μm), respectively. Therefore, the silicon carbide size for the highest energy storage efficiency was 370 μm. The experimental results imply that we may be able to target which medium to heat up between solids and gas by altering the particle size in the fluidized bed. As follow-up study, additional solar heat fluidized bed experiments are to be conducted with a mixture of solids of different particle sizes or solids with actual particle size distribution (PSD), and the results are to be analyzed in comparison to the present research outcomes obtained from the system of the single particle size.

Funding:

This paper was supported by research funds from the National Research Foundation of Korea funded by the Ministry of Education, Science and Technology (NRF-2020R1I1A3A04037715) and the Institute of Information

& communications Technology Promotion (IITP) grant funded by the Korea government (MSIT) (2021-0-02129).

Conflicts of Interest:

The authors declare no conflict of interest. The funders had no role in the design of the study; in the collection, analyses, or interpretation of data; in the writing of the manuscript, or in the decision to publish the results.

Reference

1. Guo S, Liu Q, Sun J, Jin H (2018) A review on the utilization of hybrid renewable energy. Renew Sustain Energy Rev 91:1121-1147. https://doi.org/10.1016/j.rser.2018.04.105

2. Ling JLJ, Go ES, Park YK, Lee SH (2022) Recent advances of hybrid solar-biomass thermo-chemical conversion systems. Chemosphere 290:133245. https://doi.org/10.1016/j.chemosphere.2021.133245

3. Lee SH, Lee TH, Jeong SM, Lee JM (2019) Economic analysis of a 600MWe ultra supercritical circulating fluidized bed power plant based on coal tax and biomass co-combustion plans. Renew Energy 138:121-127. https://doi.org/10.1016/j.renene.2019.01.074

4. Gwak YR, Kim YB, Gwak IS, Lee SH (2018) Economic evaluation of synthetic ethanol production by using domestic biowastes and coal mixture. Fuel 213:115-122. https://doi.org/10.1016/j.fuel.2017.10.101

5. Chen H, Zhao L, Cong H, Li X (2021) Robust solar-energy system design and optimisation for reactive distillation column in methyl acetate hydrolysis process. Energy Convers Manag 243:114426. https://doi.org/10.1016/j.enconman.2021.114426

6. Li B, Li Y, Zhang W, Qian Y, Wang Z (2020) Simultaneous NO/SO2 removal by coconut shell char/CaO from calcium looping in a fluidized bed reactor. Korean J Chem Eng 37:688-697. https://doi.org/10.1007/s11814-020-0483-8

7. Zhao Y, Dunn A, Lin J, Shi D (2019) Photothermal effect of nanomaterials for efficient energy application. In Wang X and Chen X (ed) Novel Nanomaterials for Biomedical, Environmental and Energy Applications. Elsevier, Amsterdam, pp 415-434

8. Terme Turmo A (2017) Concentrated solar in a fluidized bed. Dissertation, Universitat Politècnica de Catalunya

9. Kearney D, Herrmann U, Nava P, Kelly B, Mahoney R, Pacheco J, Cavle R, Potrovitza N, Blake D, Price H (2003) Assessment of a molten salt heat transfer fluid in a parabolic trough solar field. J Sol Energy Eng 125: 170-176. https://doi.org/10.1115/1.1565087

10. Ho CK (2016) A review of high-temperature particle receivers for concentrating solar power. Appl Therm Eng 109:958-969. https://doi.org/10.1016/j.applthermaleng.2016.04.103

11. Calderón A, Barreneche C, Palacios A, Segarra M, Prieto C, Rodriguez- Sanchez A, Fernández AI (2019) Review of solid particle materials for heat transfer fluid and thermal energy storage in solar thermal power plants. Energy Storage 1(4):e63. https://doi.org/10.1002/est2.63

12. Nie F, Cui Z, Bai F, Wang Z (2019) Properties of solid particles as heat transfer fluid in a gravity driven moving bed solar receiver. Sol Energy Mater Sol Cells 200:110007. https://doi.org/10.1016/j.solmat.2019.110007

13. Upadhyay M, Seo MW, Naren PR, Park JH, Nguyen TDB, Rashid K, Lim H (2020) Experiment and multiphase CFD simulation of gas-solid flow in a CFB reactor at various operating conditions: Assessing the performance of 2D and 3D simulations. Korean J Chem Eng 37:2094-2103. https://doi.org/10.1007/s11814-020-0646-7

14. Gwak YR, Yun JH, Keel SI, Lee SH (2020) Numerical study of oxy-fuel combustion behaviors in a 2MWe CFB boiler. Korean J Chem Eng 37:1878-1887. https://doi.org/10.1007/s11814-020-0611-5

15. Gwak IS, Hwang JH, Sohn JM, Lee SH (2017) Economic evaluation of domestic biowaste to ethanol via a fluidized bed gasifier. J Ind Eng Chem 47:391-398. https://doi.org/10.1016/j.jiec.2016.12.010

16. Kang SY, Go ES, Seo SB, Kim HW, Keel SI, Lee SH (2021) A comparative evaluation of recarbonated $CaCO_3$ derived from limestone under oxy-fuel circulating fluidized bed conditions. Sci Total Environ 758:143704. https://doi.org/10.1016/j.scitotenv.2020.143704

17. Park SH, Kim SW (2021) Characteristics of Heat Absorption by Gas in a Directly-irradiated Fluidized Bed Particle Receiver. Korean Chem Eng Res 59:239-246. https://doi.org/10.9713/kcer.2021.59.2.239

18. Gokon N, Takahashi S, Yamamoto H, Kodama T (2008) Thermochemical two-step water-splitting reactor with internally circulating fluidized bed for thermal reduction of ferrite particles. Int J Hydrog Energy 33:2189-99. https://doi.org/10.1016/j.ijhydene.2008.02.044

19. Alonso E, Romero M (2015) Review of experimental investigation on directly irradiated particles solar reactors. Renew Sustain Energy Rev 41:53-67. https://doi.org/10.1016/j.rser.2014.08.027

20. Briongos JV, Gómez-Hernández J, González-Gómez PA, Serrano D (2018) Two-phase heat transfer model of a beam-down gas-solid fluidized bed solar particle receiver. Sol Energy 171:740-50. https://doi.org/10.1016/j.solener.2018.07.016

21. Díaz-Heras M, Calderón A, Navarro M, Almendros-Ibáñez JA, Fernández AI, Barreneche C (2021) Characterization and testing of solid particles to be used in CSP plants: Aging and fluidization tests. Sol Energy Mater Sol Cells 219:110793. https://doi.org/10.1016/j.solmat.2020.110793

22. Nie F, Yu Y, Bai F, Wang Z (2020) Experimental and numerical investigation on thermal performance of a quartz tube solid particle solar receiver. Sol Energy 207:1055-1069. https://doi.org/10.1016/j.solener.2020.07.013

23. Kang SY, Seo SB, Go ES, Kim HW, Keel SI, Park YK, Lee SH (2021) Effect of particle size on in-situ desulfurization for oxy-fuel CFBC. Fuel 291:120270. https://doi.org/10.1016/j.fuel.2021.120270

24. Kunii L, Levenspiel O (1991) Fluidization Engineering. Butterworth-Heinemann, Massachusetts USA

25. Kim HW, Lee D, Nam H, Hong YW, Seo SB, Go ES, Lee SH (2020) Attrition and Heat Transfer Characteristics of Fluidized Bed Materials for a Solar Hybrid Process. Clean Technology 26(1):65-71. https://doi.org/10.7464/ksct.2020.26.1.65

26. Díaz-Heras M, Barreneche C, Belmonte JF, Calderón, A, Fernández AI, Almendros-Ibáñez JA (2020) Experimental study of different materials in fluidized beds with a beam-down solar reflector for CSP applications. Sol Energy 211:683-699. https://doi.org/10.1016/j.solener.2020.07.011

27. Sih SS, Barlow JW (2004) The prediction of the emissivity and thermal conductivity of powder beds. Particul Sci Technol 22(4):427-440. https://doi.org/10.1080/02726350490501682

28. Díaz-Heras M, Moya JD, Belmonte JF, Córcoles-Tendero JI, Molina AE, Almendros-Ibáñez JA (2020) CSP on fluidized particles with a beam-down reflector: Comparative study of different fluidization technologies. Sol Energy 200:76-88. https://doi.org/10.1016/j.solener.2019.09.006

29. Liu Q, Bai Z, Wang X, Lei J, Jin H (2016) Investigation of thermodynamic performances for two solar-biomass hybrid combined cycle power generation systems. Energy Convers Manag 122:252-262. https://doi.org/10.1016/j.enconman.2016.05.080

30. Kim MJ, LeeKM, Bak YS, Lee JM (2021) A two-way coupled CFD-DQMOM approach for long-term dynamic simulation of a fluidized bed reactor. Korean J Chem Eng 38:342-353. https://doi.org/10.1007/s11814-020-0701-4

31. Flamant G (1982) Theoretical and experimental study of radiant heat transfer in a solar fluidized- bed receiver. AIChE J 28(4):529-535. https://doi.org/10.1002/aic.690280402

32. Matsubara K, Kazuma Y, Sakurai A, Suzuki S, Soon-Jae L, Kodama T, Yoshida K (2014) High-temperature fluidized receiver for concentrated solar radiation by a beam-down reflector system. Energy Procedia 49:447-456. https://doi.org/10.1016/j.egypro.2014.03.048

Table 1. Physical properties of sand, SiC, Al

Property	**Sand**	**SiC**	**Al**
Mean size (μm)	182	315	310
Melting point (℃)	1903	2730	2072
Boiling point (℃)	2590	N/A	2977
Molecular wt (g/mol)	60.08	40.11	101.96
Density (g/cm^3)	2.17-2.65	3.0-3.2	3.4-4.1
Hardness (MPa)	4500-9500	15710	25500
Poisson's ratio (-)	0.17	0.15-0.21	0.22-0.24
Compressive strength (MPa)	1100-1600	2780-3900	1920-2750
Elastic modulus (GPa)	73	370-490	220-370
Specific heat capacity (J/kgK)	480-730	670-1180	870-940
Thermal conductivity (W/mK)	1.3-1.5	120-170	14-30
Thermal expansion (10^{-6}/K)	0.55-0.75	4.0-4.5	6.7-8.2
Emissivity (-)	0.49	0.9	0.85
Attrition (%)	9.3	7.8	6.2

Table 2. Specific heat of solid particles and air

Particle	**Cp (kcal/kg.℃)**
Sand	0.2
SiC	0.25
Al	0.197
Air	0.24

Figure

List of Figures

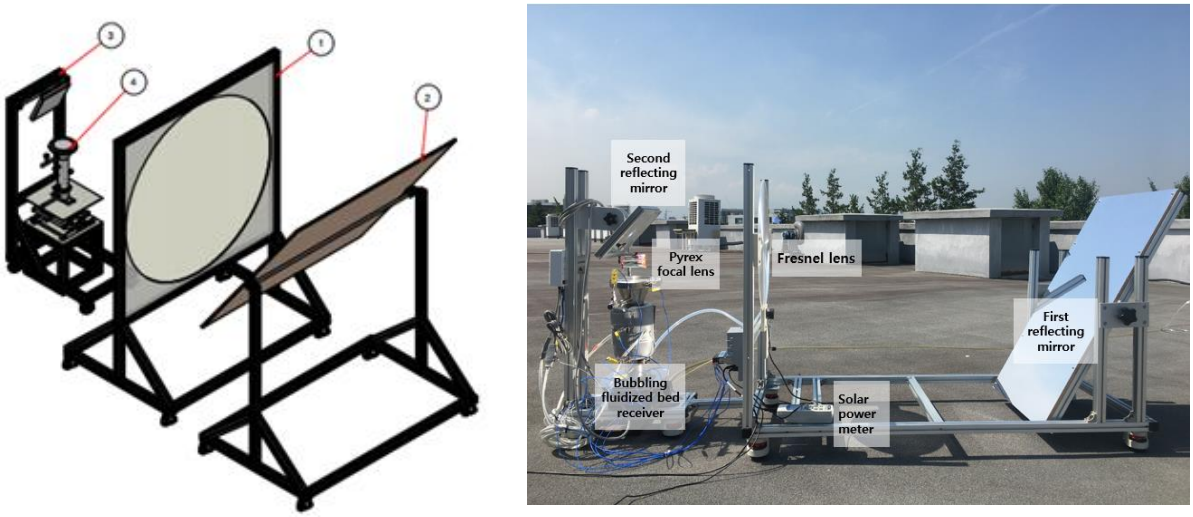

Fig. 1 Configuration of overall system

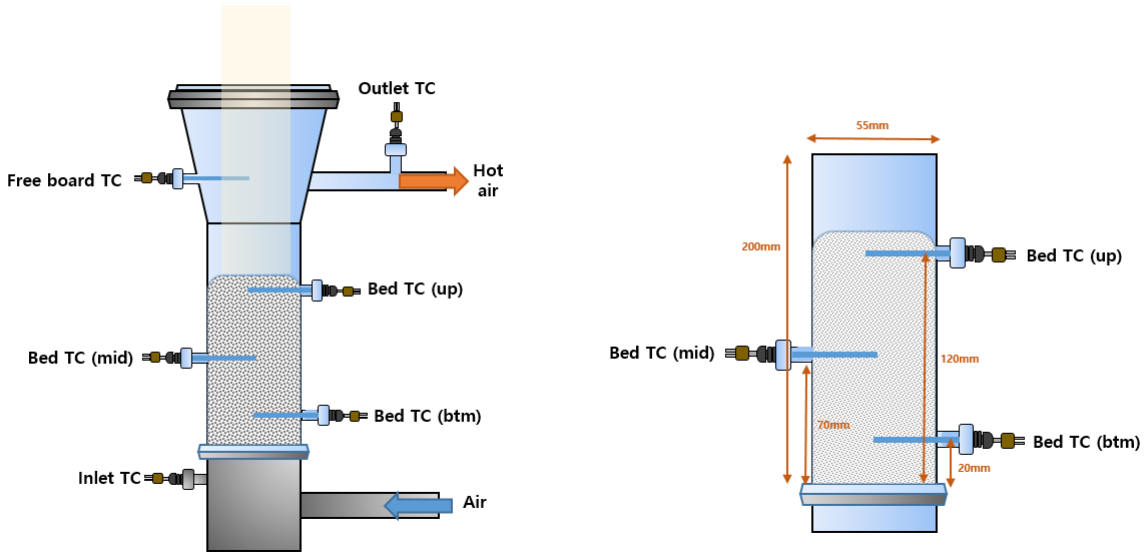

(a) (b)

Fig. 2 Bubbling fluidized bed receiver

Fig. 3 Overall system configuration of the upscale equipment

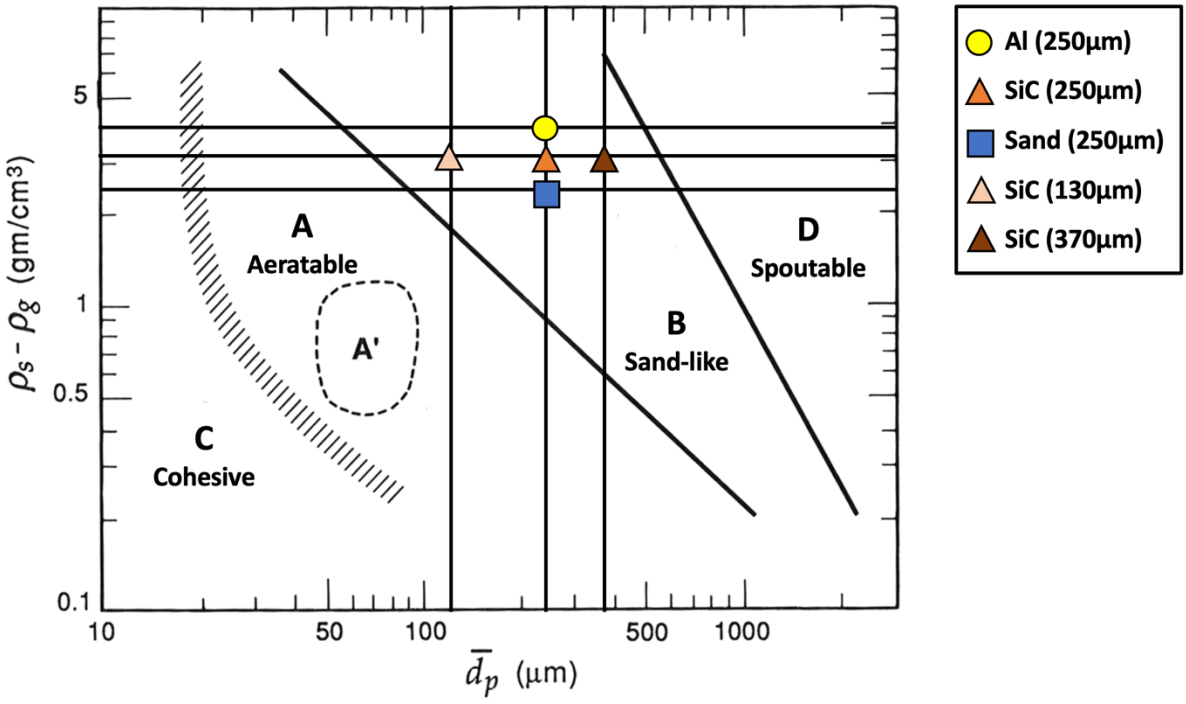

Fig. 4 Classification of solar thermal material [18]

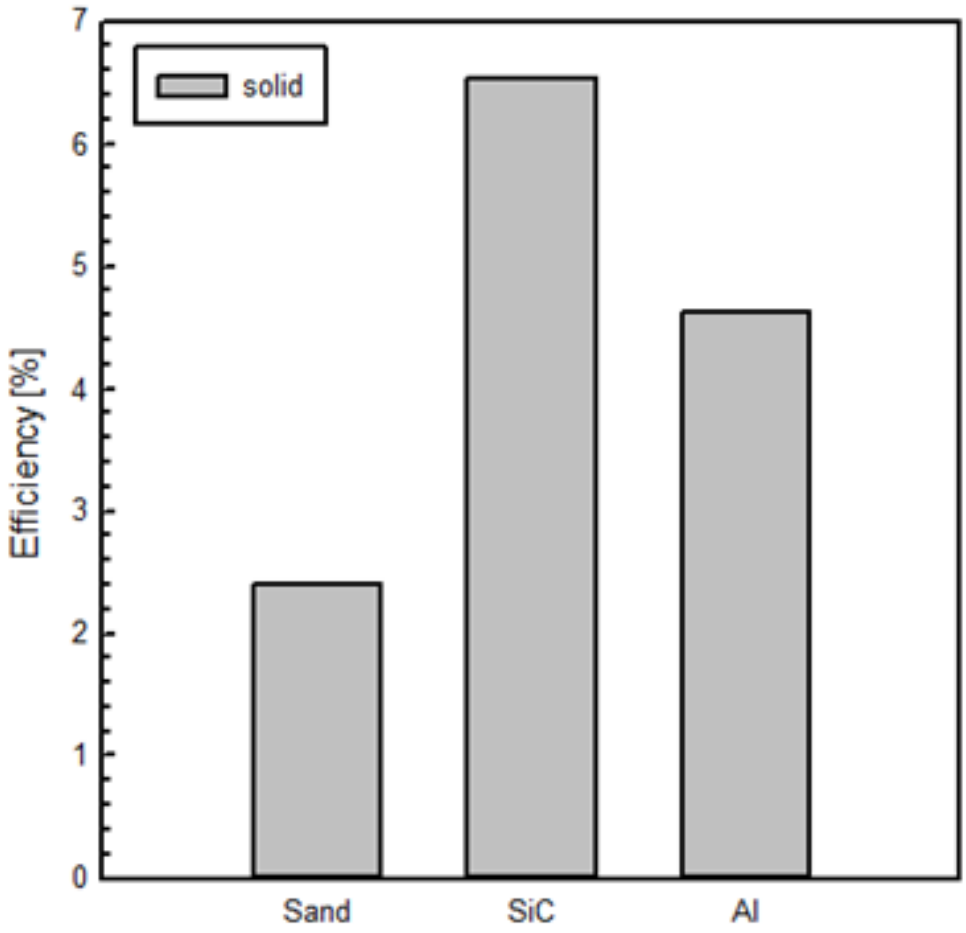

Fig.5 Thermal efficiency of the receiver with energy stored in particle

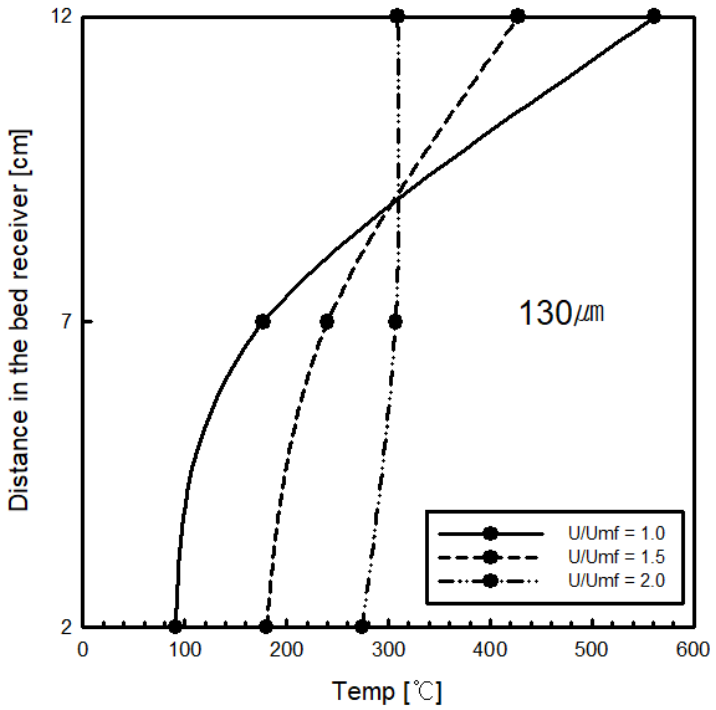

(a)

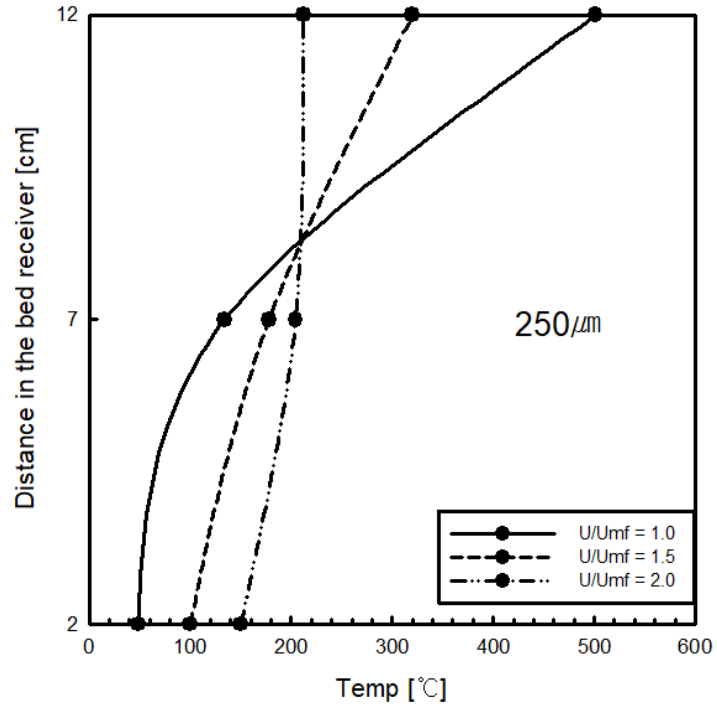

(b)

Fig. 6 Axial temperature profiles of a bubble fluidized bed with different SiC particle sizes; (a) 130 μm, (b) 250 μm

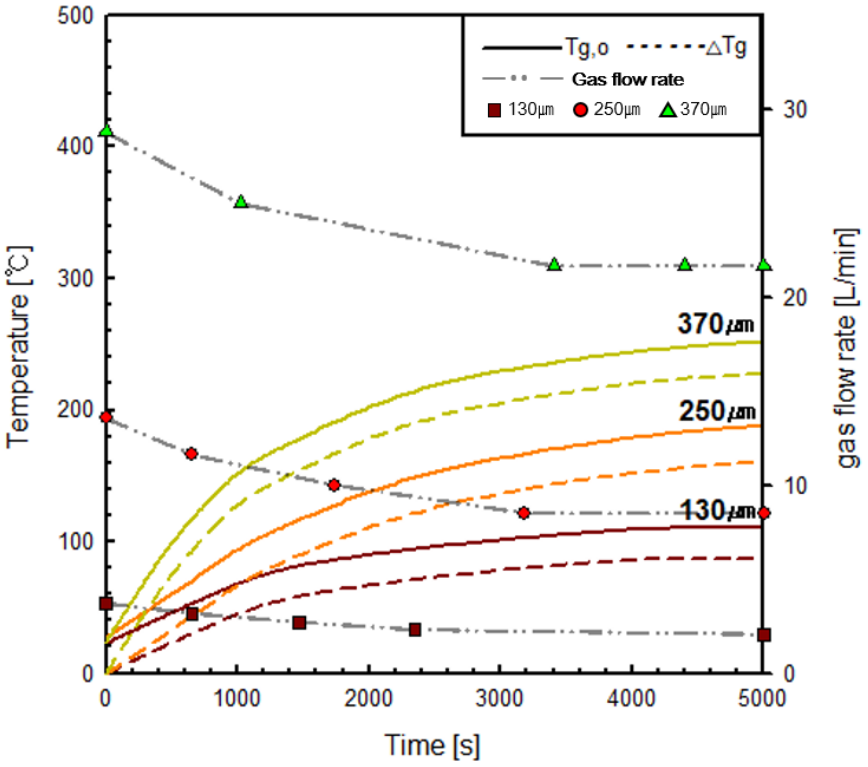

(a)

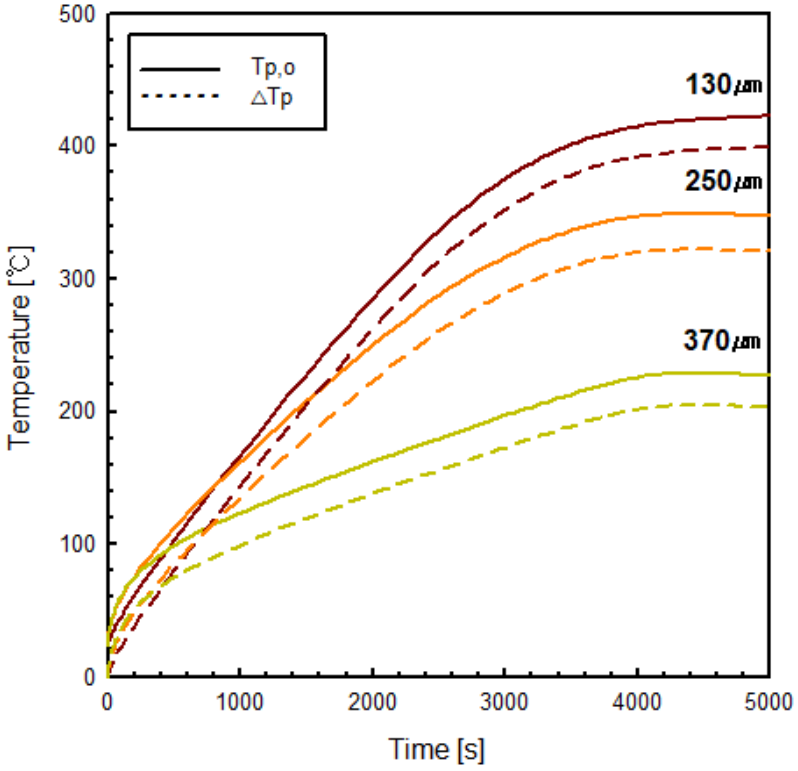

(b)

Fig. 7 Temperature change by particle size at 1.5 Umf for 5000 s; (a) gas (b) particle

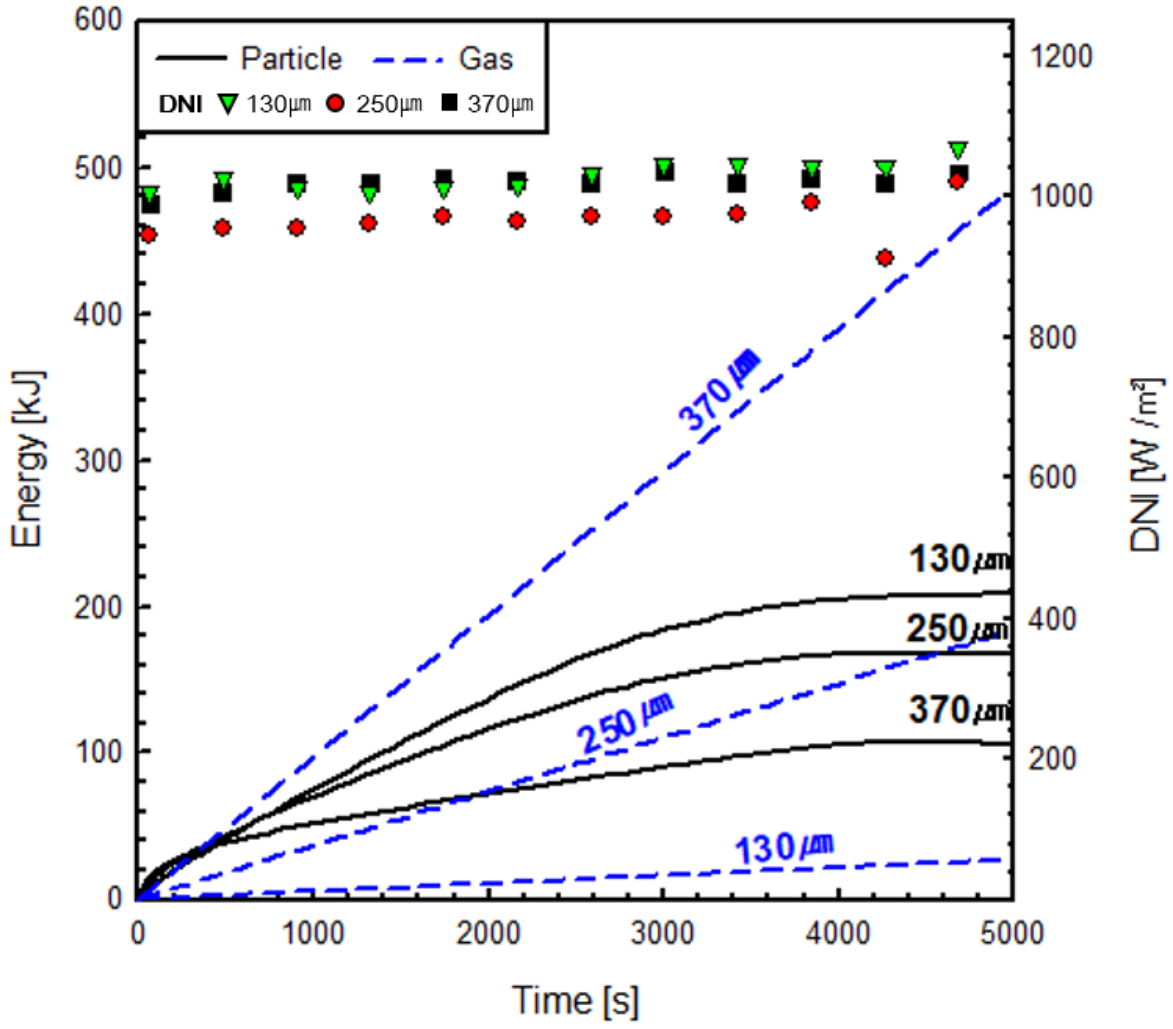

Fig. 8 Energies stored in the particle or carried by the gas stream for different particle sizes

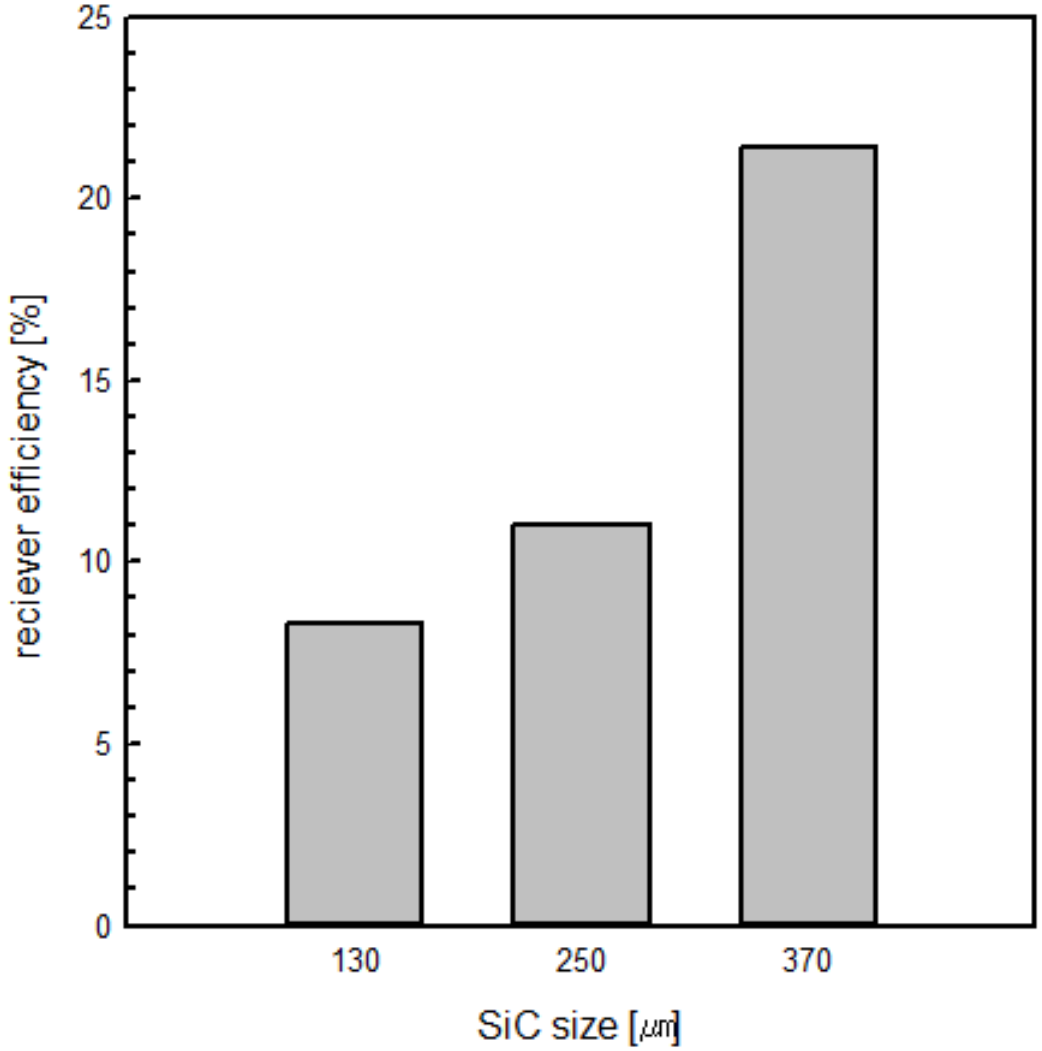

Fig. 9 Comparison of receiver efficiency according to particle size (1.5 Umf)

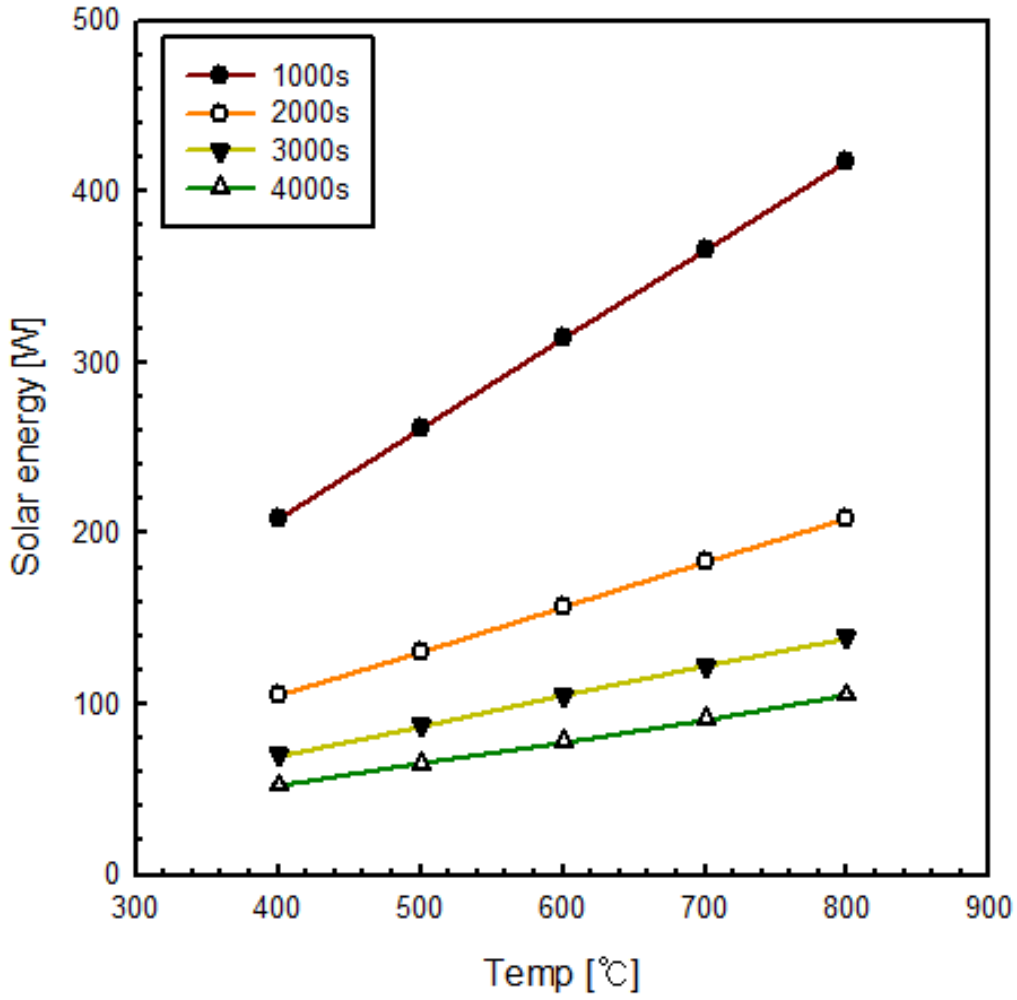

Fig. 10 Solar energy based on target temperature and cumulative exposure time of sunbeams to particles